"HOT" NON-FLARING PLASMA IN ACTIVE REGIONS II. IMPACTS OF TWO-FLUID EFFECTS

W. T. Barnes and S. J. Bradshaw
Department of Physics & Astronomy, Rice University, Houston, TX 77251-1892

P. J. Cargill
Space and Atmospheric Physics, The Blackett Laboratory, Imperial College, London SW7 2BW and
School of Mathematics and Statistics, University of St. Andrews, St. Andrews, Scotland KY16 9SS
Draft version September 29, 2015

ABSTRACT

Faint, high-temperature emission in active region cores has long been predicted as a signature of nanoflare heating. However, the detection of such emission has proved difficult due to a combination of the efficiency of thermal conduction, non-equilibrium ionization, and inadequate instrument sensitivity. This second paper in our series on hot non-flaring plasma in active regions aims to show how the assumption of electron-ion equilibrium in hydrodynamic models leads to incorrect conclusions regarding the hot emission. We have used an efficient two-fluid hydrodynamic model to carry out a parameter exploration in preferentially heated species, nanoflare heating frequency, and event amplitude power-law index. By computing the emission measure distributions and calculating their "hotward" slopes, we have concluded that the assumption of electron-ion equilibrium leads to an understimate of the amount of hot plasma at intermediate and high heating frequencies. Additionally, in the single-fluid approximation, hot emission measure slopes show only a very weak dependence on heating frequency while in the electron-only heating scenario, the hotward slope varies more as the heating frequency increases.

1. INTRODUCTION

Need to reword this introduction; move from introduction of hot plasma as signature of nanoflares to observational evidence for nanoflares and why it is hard to come by; to models which show evidence of nanoflares; to what we will do in this paper

Cargill (1994); Cargill & Klimchuk (2004) have predicted that emission measure distributions resulting from nanoflare models should be wide and have a faint, high-temperature ($> 4 \times 10^6$ K) component and thus a steep hotward slope. Unfortunately, observing this high-temperature emission is difficult and in some cases impossible. The reason for this difficulty is twofold. First, thermal conduction is a very efficient cooling mechanism at high temperatures and large spatial temperature gradients. Thus, because the increase in density lags the increase in temperature due to heating and because EM $\propto n^2$, by the time sufficient densities are acheived, the plasma has cooled down such that the fingerprints of nanoflare heating have been smoothed out.

The second reason for this difficulty is non-equilibrium ionization. It is usually assumed that the observed line intensities, because of their known formation temperatures, are a direct indicator of the plasma temperature. However, if the heating timescale is shorter than the ionization timescale, the time it takes for the ion population to settle into the correct charge state, an equilibrium assumption can lead to a misdiagnosis of the plasma temperature. This makes signatures of hot, nanoflare-heated plasma especially difficult to detect if the high temperatures persist for less than the ionization timescale (Bradshaw & Cargill 2006; Bradshaw & Klimchuk 2011; Reale

will.t.barnes@rice.edu

& Orlando 2008).

Despite these difficulties, various attempts have been made to observe this faint high-temperature emission. Using the broadband X-Ray Telescope (XRT) aboard the *Hinode* spacecraft, Schmelz et al. (2009) and Reale et al. (2009) show a faint hot component in the reconstructed DEM curves. However, since the channels on such broadband instruments can often be polluted by low-temperature emission, the reliability of such measurements depends on the filtering technique used. Additionally, Winebarger et al. (2012) showed that combinations of *Hinode*/EIS and *Hinode*/XRT measurements leave a "blind spot" in the EM$-T$ space coinincident with where evidence for nanoflare heating is likely to be found. Unambiguous observational evidence of nanoflare heating must come from pure spectroscopic measurements (see Brosius et al. 2014). Missions like the Marshall Grazing Incidence X-ray Spectrometer (MaGIXS) (Kobayashi et al. 2011; Winebarger 2014), with a wavelength range of 6-24 Å and a temperature range of $6.2 < \log T < 7.2$, aim to probe this previously poorly-resolved portion of the coronal spectrum in hopes of better quantifying the presence of faint, high-temperature plasma.

The Parker nanoflare concept has become one of the most favored and contentious coronal heating models (Cargill 1994; Cargill & Klimchuk 2004; Klimchuk 2006). While many theoretical efforts (e.g. Bradshaw et al. 2012; Reep et al. 2013) have shown the feasability of nanoflares, the idea has long suffered from a lack observational evidence, though recent high-resolution and high-cadence observations (Brosius et al. 2014; Testa et al. 2013, 2014) have provided encouraging results. The term *nanoflare* has now become synonymous with impulsive heating in the energy range $10^{24} - 10^{27}$ ergs, with no specific as-

sumption as to what underlying physical mechanism is responsible for this heating. Thus, in this work, the term nanoflare will refer to bursty energy release on a timescale of approximately 100 s or less.

Need paragraph here saying something about two-fluid approach: why is it important in nanoflare heating scenarios?

Wouldn't be a bad idea to include summary of measured "hotward" emission slope values as is done in Bradshaw et al. (2013) for cool slopes

In this paper, the second in our series on hot emission in active region cores, we will use an efficient two-fluid hydrodynamic model to explore the effect of electron and ion heating on nanoflare-heated loops. In particular, we will look at how the hot emission is affected by heating preferentially one species or the other as well as how this hot emission can vary with heating frequency, loop length, and event amplitude power-law index. We will make comparisons to results from single-fluid models in an effort to diagnose how the assumption of electron-ion equilibrium can affect conclusions about this hot emission, the so-called "smoking gun" of nanoflare heating.

2. NUMERICAL MODEL

1D hydrodynamic models are excellent tools for computing field-aligned quantities in coronal loops. However, because of the small grid sizes needed to resolve the transition region and consequently small timesteps needed to resolve thermal conduction, the use of such models in large parameter sweeps is made impractical by long runtimes (Bradshaw & Cargill 2013). Thus, in our numerical study, we will use a modified form of the popular 0D enthalpy-based thermal evolution of loops (EBTEL) model (Klimchuk et al. 2008; Cargill et al. 2012a,b, 2015) which computes time-dependent spatially-averaged loop quantities and has been successfully benchmarked against the 1D HYDRAD code (Bradshaw & Cargill 2013).

We have modified the usual EBTEL equations (see Cargill et al. 2012a) to treat the evolution of the electron and ion populations separately while maintaining the assumption of quasi-neutrality, $n_e = n_i = n$. This amounts to computing spatial averages of the two-fluid hydrodynamic equations over both the transition region and corona. We will reserve a full discussion of this modified EBTEL model for a future paper. The modified two-fluid EBTEL equations are,

$$\frac{d}{dt}\bar{p}_e = \frac{\gamma - 1}{L}[\psi_{TR} + \psi_C - (\mathcal{R}_{TR} + \mathcal{R}_C)] +$$
$$k_B\bar{n}\nu_{ei}(\bar{T}_i - \bar{T}_e) + (\gamma - 1)\bar{E}_{H,e}, \quad (1)$$

$$\frac{d}{dt}\bar{p}_i = -\frac{\gamma - 1}{L}(\psi_{TR} + \psi_C) + k_B\bar{n}\nu_{ei}(\bar{T}_e - \bar{T}_i) +$$
$$(\gamma - 1)\bar{E}_{H,i}, \quad (2)$$

$$\frac{d\bar{n}}{dt} = \frac{c_2(\gamma - 1)}{c_3\gamma Lk_B\bar{T}_e}(\psi_{TR} - F_{e,0} - \mathcal{R}_{TR}), \quad (3)$$
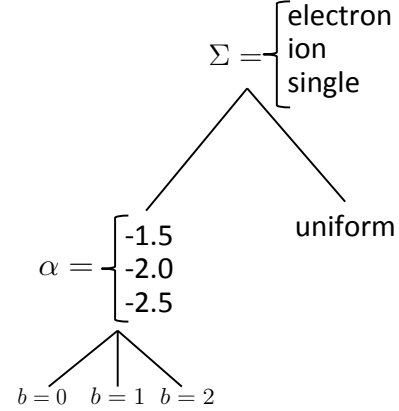
Figure 1. Parameter space covered for each loop half-length L. α is the power-law index and b indicates the scaling in the relationship $Q \propto T_N^b$, where $b = 0$ corresponds to the case where T_N and the event energy are independent.

where

$$\psi_{TR} = \frac{1}{1 + \xi}(F_{0,e} + \mathcal{R}_{TR} - \xi F_{0,i}), \quad (4)$$

$$\psi_C = = \bar{v}p_e^{(a)} - (p_e v)_0. \quad (5)$$

Additionally, Eqs. 1, 2, and 3 are closed by the equations of state $p_e = k_B n T_e$ and $p_i = k_B n T_i$.

The volumetric heating rates, $E_{H,e}$ and $E_{H,i}$, are the primary degrees of freedom in our model. In the case of electron (ion) heating, $E_{H,i}(E_{H,e}) = 0$. $\bar{p}_e, \bar{p}_i$ and $\bar{T}_e, \bar{T}_i$ are the spatially-averaged coronal electron and ion pressures and temperatures, respectively and $\bar{n}$ is the spatially-averaged coronal number density. $\mathcal{R}_C = \bar{n}^2\Lambda(\bar{T})$ is the volumetric coronal radiative loss rate, where $\Lambda(\bar{T})$ is the radiative loss function, and $\mathcal{R}_{TR} = c_1\mathcal{R}_C$ is the radiative loss rate in the transition region where the calculation of c_1 is described in Cargill et al. (2012a). Additionally, $F_{e,0}, F_{i,0}$ are the electron and ion conductive fluxes as computed at the base of the loop, respectively, and are calculated using the classical Spitzer formula with a flux limiter imposed to prevent runaway cooling at low densities. The Coulomb collision frequency, ν_{ei}, is given by,

$$\nu_{ei} = \frac{16\sqrt{\pi}}{3}\frac{e^4}{m_e m_i}\left(\frac{2k_B\bar{T}_e}{m_e}\right)^{-3/2}\bar{n}\ln\Lambda, \quad (6)$$

where m_e, m_i are the electron and ion masses respectively and $\ln\Lambda$ is the Coulomb logarithm. Finally, $c_2 = \bar{T}/T_a = 0.6$, $c_3 = T_0/T_a = 0.9$, determined by static equilibrium, and $\xi = \bar{T}_e/\bar{T}_i$.

Note that in the limit that $\bar{T}_e = \bar{T}_i$ such that $\xi = 1$, Eq. 3 reduces to the single-fluid density equation of Cargill et al. (2012a). Additionally, Eqs. 1 and 2 can be added together to recover the single-fluid pressure equation. As with the original EBTEL model, the modified two-fluid version has been successfully benchmarked against the HYDRAD hydrodynamic code.

3. PARAMETER SPACE

Talk about heating functions; varying heating frequency; energy budget; MC runs
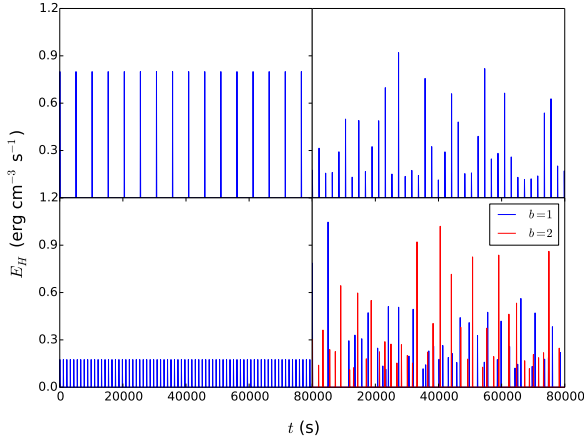
Figure 2. All heating functions are for $L = 40$ Mm. Starting counter-clockwise from the bottom left: uniform heating amplitudes for $T_N = 1000$ s; uniform heating amplitudes for $T_N = 5000$ s; power-law distributed heating amplitudes for $\alpha = -1.5$, $T_N = 2000$ s; power-law distributed amplitudes for $\alpha = -1.5$ where the wait times depend on the event energies and the mean wait time for both b values is $\langle T_N \rangle = 2000$ s.

4. RESULTS

4.1. *Electron Heating*

4.2. *Ion Heating*

4.3. *Single-fluid*

5. DISCUSSION

6. CONCLUSION

REFERENCES

Bradshaw, S. J., & Cargill, P. J. 2006, Astronomy and Astrophysics, 458, 987
—. 2013, The Astrophysical Journal, 770, 12
Bradshaw, S. J., & Klimchuk, J. A. 2011, The Astrophysical Journal Supplement Series, 194, 26
Bradshaw, S. J., Klimchuk, J. A., & Reep, J. W. 2012, The Astrophysical Journal, 758, 53
Brosius, J. W., Daw, A. N., & Rabin, D. M. 2014, The Astrophysical Journal, 790, 112
Cargill, P. J. 1994, The Astrophysical Journal, 422, 381
Cargill, P. J., Bradshaw, S. J., & Klimchuk, J. A. 2012a, The Astrophysical Journal, 752, 161
—. 2012b, The Astrophysical Journal, 758, 5
Cargill, P. J., & Klimchuk, J. A. 2004, The Astrophysical Journal, 605, 911
Cargill, P. J., Warren, H. P., & Bradshaw, S. J. 2015, Phil. Trans. R. Soc. A, 373, 20140260
Klimchuk, J. A. 2006, Solar Physics, 234, 41
Klimchuk, J. A., Patsourakos, S., & Cargill, P. J. 2008, The Astrophysical Journal, 682, 1351
Kobayashi, K., Cirtain, J., Golub, L., et al. 2011, in Society of Photo-Optical Instrumentation Engineers (SPIE) Conference Series, Vol. 8147, 81471M
Reale, F., & Orlando, S. 2008, The Astrophysical Journal, 684, 715
Reale, F., Testa, P., Klimchuk, J. A., & Parenti, S. 2009, The Astrophysical Journal, 698, 756
Reep, J. W., Bradshaw, S. J., & Klimchuk, J. A. 2013, The Astrophysical Journal, 764, 193
Schmelz, J. T., Saar, S. H., DeLuca, E. E., et al. 2009, The Astrophysical Journal Letters, 693, L131
Testa, P., De Pontieu, B., Martnez-Sykora, J., et al. 2013, The Astrophysical Journal Letters, 770, L1
Testa, P., De Pontieu, B., Allred, J., et al. 2014, Science, 346, 1255724
Winebarger, A. R. 2014, AGU Fall Meeting Abstracts, 52, 03
Winebarger, A. R., Warren, H. P., Schmelz, J. T., et al. 2012, The Astrophysical Journal Letters, 746, L17